X-ray photoelectron characterization of 6*H*-SiC(0001)

L. Simon,* J. L. Bischoff, and L. Kubler
Laboratoire de Physique et de Spectroscopie Electronique, UPRES. A CNRS 7014, Faculté des Sciences et Techniques, 4, rue des Frères Lumière, 68093 Mulhouse Cedex, France
(Received 12 March 1999; revised manuscript received 16 July 1999)

X-ray photoelectron spectroscopy and photoelectron-diffraction (XPD) measurements are performed on 6*H*-SiC(0001) for three different reconstructed surfaces: one Si-rich 3×3 and two C-rich $\sqrt{3}\times\sqrt{3}R30°$ and $6\sqrt{3}\times6\sqrt{3}R30°$ reconstructed surfaces. In each case, the C 1*s* and Si 2*p* core-level lines are shown and XPD patterns are compared with double-scattering calculations of an ideal unreconstructed surface. No significant differences have been observed in the experimental C 1*s* and Si 2*p* *bulk* component XPD patterns with the changes of the surface reconstruction. These experimental XPD patterns fit the simulations of an unreconstructed model fairly well. For the highly C-rich $6\sqrt{3}\times6\sqrt{3}R30°$ reconstructed surface, XPD patterns of the different deconvoluted components of the C 1*s* core line are presented. An agreement between the experimental C 1*s* *surface* component XPD diagram and calculations allows us to propose a model for this reconstruction based on Si adatoms at T_4 sites covered by a commensurable graphite top layer. [S0163-1829(99)09739-8]

I. INTRODUCTION

Silicon carbide provides a lot of interesting properties such as a wide band gap, a large electron mobility, as well as high physical and chemical stability. It will, therefore, be widely used in high-temperature and high power applications.[1] Most of the silicon carbide polytypes studied are the hexagonal form named α (principally 4*H* and 6*H*-SiC), and the cubic form named β or 3*C*-SiC. We focus here on the 6*H* polytype. 6*H*-SiC crystallographic structure consists of the stacking of Si-C bilayers with an *ABCACBA* sequence along the *c* (or *z*) axis ($\langle0001\rangle$ directions) of the hexagonal structure, where each letter (*A*, *B*, and *C*) corresponds to a Si-C bilayer. The 6*H*-SiC(0001) surface provides several reconstructions depending on the surface preparation. Starting with a usual 1×1 oxidized surface, an ultrahigh vacuum (UHV) annealing (above 1000 °C) removes the residual surface oxide, but leads to a carbon enrichment of the surface due to Si desorption from the substrate. As evidenced by a lot of authors,[2–6] a $\sqrt{3}\times\sqrt{3}R30°$ reconstruction results from this cleaning procedure. In order to avoid silicon desorption, the common procedure which consists in annealing at lower temperature (850 °C) under a silicon flux leads to a 3×3 reconstructed surface.[7–10] Further UHV heating ranging from 1100 °C to 1200 °C without silicon flux leads to a $\sqrt{3}\times\sqrt{3}R30°$ reconstructed surface and with subsequent heating around 1250 °C, to a higher C-enriched $6\sqrt{3}\times6\sqrt{3}R30°$ one.[7,11–14] The atomic structures of these C-rich reconstructed surfaces are still under debate.

For the $\sqrt{3}\times\sqrt{3}R30°$ reconstruction, Van Elsbergen, Kampen, and Mönch[7] have observed by Auger-electron spectroscopy (AES) that silicon atoms are still present on the top of the surface. Owman and Märtensson[10] studied this reconstruction by STM and found an atomic structure composed of $\frac{1}{3}$ layer of Si or C adatoms in threefold-symmetric on top of the outermost silicon layer. These adatoms have been theoretically identified by Northrup and Neugebauer[15] to be Si adatoms at the T_4 site. For the $\sqrt{3}\times\sqrt{3}R30°$ reconstruction associated with Si desorption and C enrichment, Forbeaux *et al.*[16] proposed a top bilayer where the Si plane is partly or fully substituted by C atoms. The latter, together with Johansson *et al.*[17] and Gunnella *et al.*[14] evidenced a semiconducting surface with a surface state at 1.2 eV below the Fermi level. Otherwise, Badziag[18] proposed a Si_2C_6 ring (where topmost atoms are silicon) distribution over the layer which can be enriched in carbon atoms in order to form C_8 clusters. His model tentatively explains the two surface components of the C 1*s* core level found by Johansson, Owman, and Märtensson[19] and a possible presence of silicon atoms in the topmost surface.

The last $6\sqrt{3}\times6\sqrt{3}R30°$ reconstruction has been less studied in the past. Historically Van Bommel, Crombeen, and Van Tooren[2] interpreted it as a graphitic layer on the topmost surface. A number of scanning tunneling microscopy (STM) studies[3,8,20] reveal graphitic structures by the presence of honeycomblike images with 6×6 or 5×5 reconstructions. This discrepancy between the $6\sqrt{3}\times6\sqrt{3}R30°$ low-energy electron diffraction (LEED) pattern and the STM reconstructions have been interpreted by Tsai *et al.*[21] as a surface mixture of partial $\sqrt{3}\times\sqrt{3}R30°$, 5×5, and 6×6 reconstructions. The latter interpreted the 6×6 reconstruction evidenced by STM as a commensurable arrangement of a graphite monolayer on the top silicon substrate top layer. Northrup and Neugebauer[15] proposed a graphite monolayer on the top of the previous highly stable $\sqrt{3}\times\sqrt{3}R30°$ reconstruction. However, up to now, no consensus with the different structural models has been found for both C-rich $\sqrt{3}\times\sqrt{3}R30°$ and $6\sqrt{3}\times6\sqrt{3}R30°$ reconstructions as well as for their relationship.

X-ray photoelectron diffraction (XPD) characterizations have been recently performed by Bischoff, Dentel, and Kubler[22] on the (0001) and (000-1) faces of 6*H*-SiC. This technique allowed these authors to determine the bulk polarity of 6*H*-SiC. Even if this pioneer study has not been extended to differently reconstructed surfaces, the relevant results did not indicate other XPD angular features than those expected for bulk contributions. More recently, King *et al.*[23] observed on different surfaces drastic XPD pattern variations

for both C 1*s* and Si 2*p* probed core levels attributed to surface reconstruction changes from 3×3 to $\sqrt{3}\times\sqrt{3}R30°$. Without performing clear examinations of the bulk SiC contribution to the XPD patterns, these authors tentatively connected these changes to different reconstruction structural models proposed in the literature.

In this paper, we wish to come back to these problems by presenting a general x-ray photoelectron spectroscopy (XPS) and x-ray photoelectron diffraction (XPD) comparison of the three 6*H*-SiC(0001) reconstructions mentioned above with the aim of knowing whether or not XPD is able to discriminate between them. To this purpose, a good knowledge of the XPD SiC bulk contribution is a prerequisite before addressing reconstruction-induced features. A particular emphasis is also given here to clearly connect the XPD patterns with well specified, i.e., either bulk or surface XPS components, selected by their different binding energies. The (10-10) and (11-20) azimuthal planes are extensively probed by XPD, whose patterns are compared with double-scattering calculations of an ideal truncated and unreconstructed bulk substrate. This procedure allows discussion and a fair understanding of the main XPD features. For the high C-rich $6\sqrt{3}\times6\sqrt{3}R30°$ reconstruction, the C 1*s* core-level peak presents different convoluted components. The XPD patterns of each component have been recorded and a structural model has been proposed for this reconstruction through simulations.

II. EXPERIMENT

6*H*-SiC(0001) single-crystals purchased from Cree, Inc. and capped with an *n*-doped epilayer are loaded in an ultrahigh vacuum preparation chamber (10^{-10} mbar). The cleaning procedure consists of an annealing at 800 °C during a few minutes under a silicon flux calibrated by a quartz microbalance (deposition rate about 7 Å/min). Samples are resistively heated and the temperature is controlled by an optical pyrometer whose emissivity is set to 0.53. This cleaning procedure removes the native oxide and other impurities and allows a 3×3 surface reconstruction observation by LEED. Further annealing at 1200 and 1250 °C without silicon flux leads to a $\sqrt{3}\times\sqrt{3}R30°$ and $6\sqrt{3}\times6\sqrt{3}R30°$ surface reconstruction, respectively.

All XPS spectra are acquired using a Mg $K\alpha$ (1253.6 eV) radiation. As the θ polar angle of the analyzed electrons can be varied by sample rotation around the sample holder axis, polar angle scans of specific core-level intensities can be achieved. These data, also named XPD angular distributions, provide surface crystallographic information. The displayed XPD modulations are collected in (10-10) and (11-20) polar planes. The solid line relating the data points is obtained using a conventional smoothing procedure. XPS curve fittings are carried out using a commercial curve processing package. The peaks are fitted by a standard Voigt function. The fit quality is checked by minimizing χ^2. Identical linewidths and the same Voigt function are imposed to all SiC components for each reconstructed surface.

III. XPS CHARACTERIZATION OF 6*H*-SiC(0001) SURFACES FOR THE DIFFERENT RECONSTRUCTIONS

Figures 1 and 2 display the C 1*s* and Si 2*p* core-level peaks, respectively, for the 3×3, $\sqrt{3}\times\sqrt{3}R30°$, and $6\sqrt{3}\times6\sqrt{3}R30°$ reconstructed surfaces. These spectra are recorded at the polar angles $\theta=0°$ (mainly sensitive to the bulk states) [Figs. 1(a), 1(c), and 1(e) and Figs. 2(a), 2(c), and 2(e)] and $\theta=50°$ (mainly sensitive to the surface states) [Figs. 1(b), 1(d), and 1(f) and Figs. 2(b), 2(d), and 2(e)].

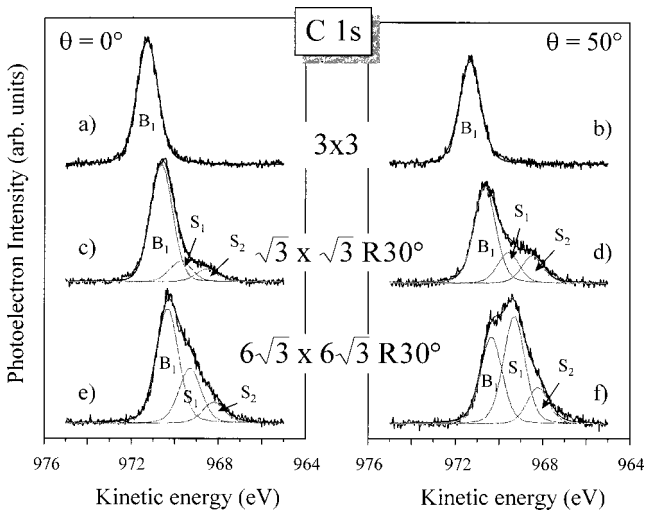

FIG. 1. C 1*s* core-level peaks recorded on 3×3 (a and b), $\sqrt{3}\times\sqrt{3}R30°$ (c and d) and $6\sqrt{3}\times6\sqrt{3}R30°$ (e and f) reconstructed surfaces at the polar angles $\theta=0°$ (left) and 50° (right).

Concerning the 3×3 surface reconstruction, the C 1*s* peak presents only one component named B_1 for the two polar angles of Figs. 1(a) and 1(b). This component obviously corresponds to the carbon atoms in the bulk environment of the 6*H*-SiC substrate. The relevant Si 2*p* peaks of Figs. 2(a) and 2(b) show two components. A dominant, named B_1, reflects the contribution of the Si bulk atoms of the substrate. The other one (S_1'), more intense for $\theta=50°$ and located at 1.2 eV towards higher kinetic energies, is attributed to Si-Si overlayer bonds and reveals a Si-enriched surface. This agrees with many previous studies.[7,24,25] A commonly admitted interpretation of the 3×3 surface reconstruction consists of distributed Si clusters extending over

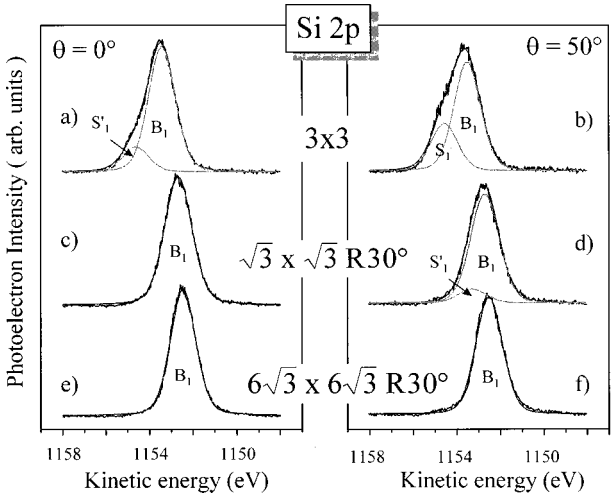

FIG. 2. Si 2*p* core-level peaks recorded on 3×3 (a and b), $\sqrt{3}\times\sqrt{3}R30°$ (c and d) and $6\sqrt{3}\times6\sqrt{3}R30°$ (e and f) reconstructed surfaces at the polar angles $\theta=0°$ (left) and 50° (right).

three monolayers of silicon atoms as experimentally evidenced by Starke *et al.*[26] and Reuter *et al.*[27] and theoretically confirmed by Badziag.[28]

After annealing at 1200 °C without Si flux during several minutes, a $\sqrt{3}\times\sqrt{3}R30°$ LEED pattern is obtained. The C 1*s* lines [Figs. 1(c) and 1(d)] now exhibit three components. The previous peak, named B_1, is energetically shifted and convoluted by two other surface components (more intense at $\theta=50°$) named S_1 and S_2. The latter components reveal a C enrichment of the surface and may correspond to C-C or Si-C bonds in a C-rich environment. For the same reconstruction, the Si 2*p* level reveals only one component at $\theta=0°$ [Fig. 2(c)]. However, the linewidth (1.5 eV) is higher than the corresponding B_1 line for the 3×3 surface (1.2 eV). This suggests the presence of a second weak component (S_1') as evidenced for a more grazing ($\theta=50°$) [Fig. 2(d)], reflecting a residue of silicon atoms at the surface.

The B_1/S_1 intensity ratio of the C 1*s* peak decreases with increasing annealing time at 1200 °C. This reflects a C-enrichment as the $\sqrt{3}\times\sqrt{3}R30°$ LEED pattern becomes brighter and is followed by the appearance of the first $6\sqrt{3}\times6\sqrt{3}R30°$ spots. However, an annealing at 1250 °C during a few minutes is necessary to obtain a well-developed $6\sqrt{3}\times6\sqrt{3}R30°$ LEED pattern without $\sqrt{3}\times\sqrt{3}R30°$ spots.

At this stage, new C 1*s* and Si 2*p* peak shapes are obtained and shown in Figs. 1(e) and 1(f) and Figs. 2(e) and 2(f). The C 1*s* peaks present the same three components seen for the previous reconstruction, but the S_1 component intensity is now more intense than the B_1 one at $\theta=50°$ [Fig. 1(f)]. The energetic positions of S_1 and S_2 components with respect to the B_1 component remained unchanged for the last two reconstructions. The Si 2*p* peaks [Figs. 2(e) and 2(f)], present only one component and the Si surface enrichment is completely suppressed.

The transition from the 3×3 to $6\sqrt{3}\times6\sqrt{3}R30°$ reconstruction is associated with a semiconductor and/or metallic transition as observed by ultraviolet photoemission spectroscopy[14] (UPS) or using synchrotron-radiation sources.[17] The presence of a density of states at the Fermi level shifts the overall peaks toward lower kinetic energies.

IV. XPD CHARACTERIZATION: 3×3 AND $\sqrt{3}\times\sqrt{3}R30°$ SURFACE RECONSTRUCTIONS

XPD is presently a well-known technique abundantly reviewed in the literature (Ref. 29 and references therein). It is a crystallographic subtechnique of XPS consisting of azimuthal or polar scans of the photoelectron intensity of specific core-level lines (C 1*s* or Si 2*p* in the present case) for monocrystalline compounds. The dominant effect of the interference process between the emitted electron wave and the waves scattered by all surrounding atoms is to provide intensity maxima along the direction of the nearest atomic neighbors of the emitter. This main effect, termed forward scattering or focusing, allows a direct angular vision of the atomic structure in real space originated from the XPS probing depth, in general, and of the nearest-neighbor direction or low index atomic rows, in particular. XPD creates a direct correlation between crystallographic atomic row directions and angular peak positions in the experimental angular distributions. This crystallographic technique also presents the advantage to be chemically selective, i.e., to probe exclusively the crystallographic environment of the emitting atom selected by the analysis of a particular XPS core level. The XPD technique was used in our group to unambiguously determine the polarity of 6*H*-SiC substrates[22] or to check the polarity and the local order of a SiO_2/6*H*-SiC interface.[30] For the SiC system, the two elements (Si or C) are well distinguished by their ''scattering power.'' The Si forward-scattering amplitude was estimated to be about twice that of the C one.[31] This fact acts directly on the forward focusing and determines the C 1*s* and Si 2*p* core-level intensities, according to the relative C and Si positions in the atomic chains.

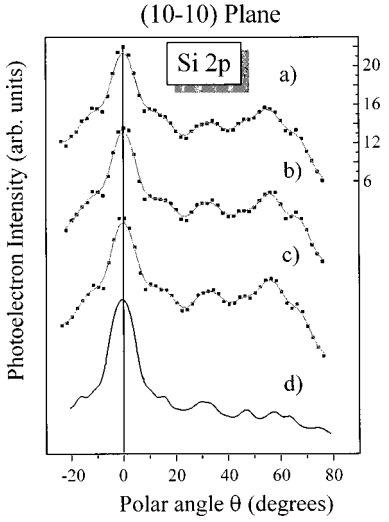

FIG. 3. XPD pattern of a Si 2*p* core-level peak (esssential contribution of the B_1 component) in the (10-10) azimuthal plane recorded on 3×3 (a), $\sqrt{3}\times\sqrt{3}R30°$ (b), and $6\sqrt{3}\times6\sqrt{3}R30°$ (c) reconstructed surfaces. Curve (d) represents a simulation of an ideal truncated 6*H*-SiC(0001) surface using a double-scattering calculation.

We now present an XPD characterization of the 6*H*-SiC monocrystal by polar angle scannings in the (11-20) and (10-10) high symmetry planes. In this study we particularly focus on finding out whether the previous varying reconstructions may generate different XPD patterns for Si 2*p* and C 1*s* bulk components. In order to understand all XPD peaks, experimental curves are compared with double-scattering calculations.

Figures 3(a)–3(c) and 4(a) and 4(b) show, respectively, the intensity modulations of the Si 2*p* and C 1*s* core-level peaks in the (10-10) plane for the 3×3 [Figs. 3(a) and 4(a)] and $\sqrt{3}\times\sqrt{3}R30°$ [Figs. 3(b) and 4(b)] reconstructions. The pass energy is set to 100 eV, and no deconvolution is carried out. In this case the intensity modulations are essentially provided by the dominant B_1 component of probed core-level lines. For the last $6\sqrt{3}\times6\sqrt{3}R30°$ reconstruction, only an experimental Si 2*p* XPD curve, recorded with pass energy of 100 eV, is shown in Fig. 3(c) but no C 1*s* one. In the latter case, the S_1 component becomes greater than B_1 and the core lines are recorded with a pass energy of 20 eV followed by deconvolutions of each peak at each polar angle. The simulations of the former XPD profiles are shown in Fig. 3*d* for Si 2*p* and in Fig. 4(c) for C 1*s*. For an ideal truncated 6*H*-SiC(0001) substrate, the atomic positions are schema-

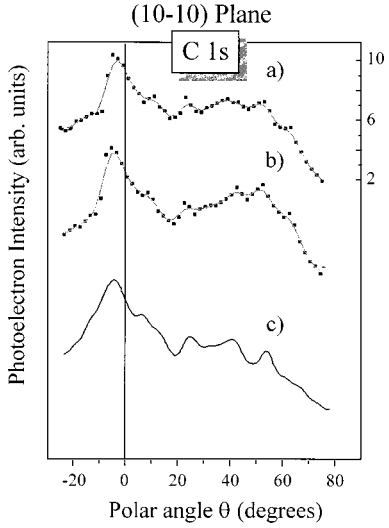

FIG. 4. XPD pattern of a C 1*s* core-level peak (essential contribution of the B_1 component) in the azimuthal plane (10-10) recorded on 3×3 (a) and $\sqrt{3}\times\sqrt{3}R30°$ (b). Simulation with a double-scattering calculation of an ideal truncated $6H$-SiC(0001) surface (c).

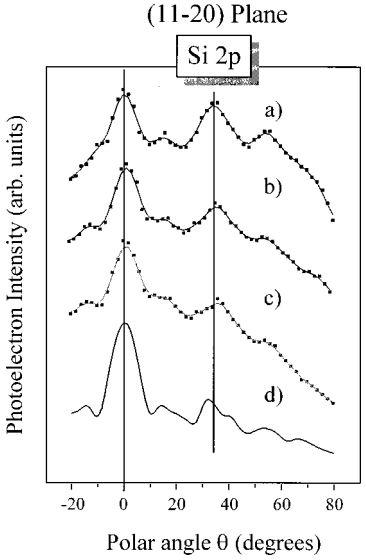

FIG. 6. XPD pattern of Si 2*p* core-level peak (essential contribution of the B_1 component) in the (10-20) azimuthal plane recorded on 3×3 (a), $\sqrt{3}\times\sqrt{3}R30°$ (b), and $6\sqrt{3}\times6\sqrt{3}R30°$ (c) reconstructed surfaces. Simulation with a double-scattering calculation of an ideal truncated $6H$-SiC(0001) surface (d).

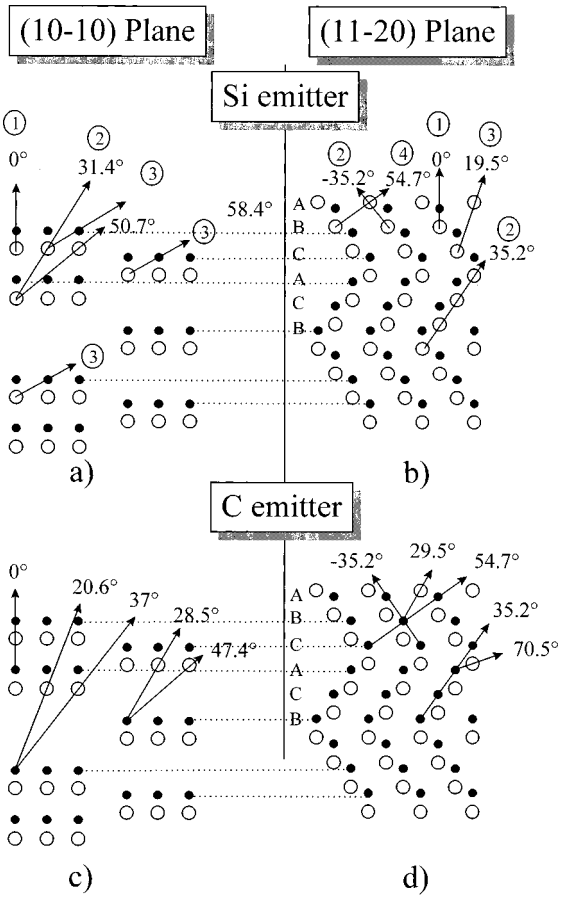

FIG. 5. (a) and (c) show a schematic of theoretical bulk crystallographic arrangements in the (11-20), and (b) and (d) the (10-10) azimuthal planes. The main forward-scattering directions are indicated by arrows for (a) and (b) carbon and (c) and (d) silicon emitters.

tized in Figs. 5(a) and 5(c) for the (10-10) azimuthal plane. They are symmetric with respect to the surface normal ($\theta=0°$) and consist of the mixing of two different atomic arrangements. The arrows indicate the main forward-scattering directions for the two types of emitters (C or Si atoms) [Figs. 5(a) and 5(c)], respectively. The XPD patterns in the (10-10) azimuthal plane (Figs. 3 and 4) are rather poorly structured. For the Si 2*p* pattern (Fig. 3), the main forward-scattering peaks are observed at $\theta=0°$, 30°, and around 58°. These structures are attributed to the directions labeled 1, 2, and 3 [Fig. 5(a)], respectively. The simulation of Fig. 3(d) reproduces the experimental XPD pattern fairly well. The similarity of patterns 3(a) to 3(c) which correspond to three different reconstructions, associated with a reasonable fit to a bulk-truncated structure, are not in favor of any reconstruction dependence of the XPD patterns, at least for our angular peak resolution ($\approx5°$).

Concerning the C 1*s* XPD profiles [Figs. 4(a) and 4(b)] we do not intend to discuss the fine structure. We can, nevertheless, note that these patterns do not depend on the surface reconstruction either and similarly for Si 2*p*, all structures are reasonably reproduced by a simulated bulk structure [Fig. 4(c)]. In this case the expected forward-scattering peak at $\theta=0°$ presents a maximum at $\theta=-5°$. This angular shift is due to our analysis geometry with a photon incidence angle of $\alpha=-35°$ which make this feature asymmetric.

Let us now focus on the XPD distribution scanned in the (11-20) azimuthal plane. The atomic arrangement in this particular azimuthal plane is shown in Figs. 5(b) and 5(d) with the bilayer stacking sequence characterizing the hexagonal structure (ABCACB). The main forward-scattering directions are indicated for both types of emitter. The Si 2*p* distributions of Figs. 6(a)–6(c) still relate to three surface reconstructions. The forward-scattering peak located at $\theta=0°$, around $\theta=35°$ and near 55° [Figs. 6(a)–6(c)] are attributed to the direction 1, 2, and 4 in Fig. 5(b). According to

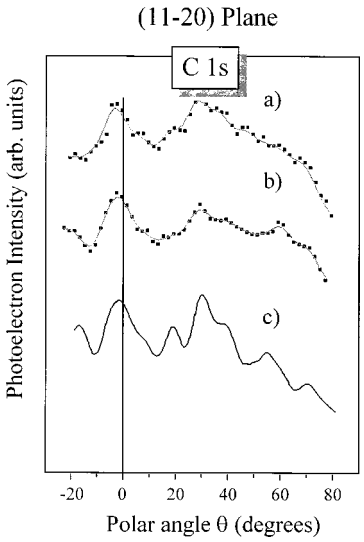

FIG. 7. C 1*s* XPD patterns (essential contribution of the B_1 component) in the (10-10) azimuthal plane recorded on 3×3 (a) and $\sqrt{3}\times\sqrt{3}R30°$ (b) reconstructed surfaces. Curve (c) is a simulation with a double-scattering calculation of an ideal truncated 6*H*-SiC(0001) surface.

the preceding observations in the (10-10) plane, they do not exhibit drastic changes with the surface reconstruction either and here again the XPD profiles are well reproduced by simulation of the bulk structure as shown by the 6*d* curve. The atomic arrangement in this plane is no longer symmetric with respect to the normal direction ($\theta=0°$). It is constituted by atomic chains alternately oriented along $\theta=35.25°$ (ACB sequence) and $\theta=-35.25°$ (ABC sequence) for each half period along the *c* axis. Therefore the first 7.5 Å (a half period along the *c* axis) under a bulk truncated surface can be formed either by ACB or ABC sequences, leading to atomic rows oriented in opposite directions with respect to the surface normal. When the polar scans are performed from $\theta=-20°$ to 80° in this azimuthal plane, a sample rotation of the azimuthal angle of 180° should theoretically provide a modified XPD signature in case of a nonequipartition of the two types of surface terminations due to either regular *c* stepping or irregular *c*/2 stepping. Nevertheless, the XPD patterns are actually not very sensitive to the termination of the substrate, i.e., the orientation of the atomic chains relative to particular ending sequences. This is due to two main reasons.

(i) The probing depth (around 60 Å) at the origin of the XPD information is too high (with respect to *c*/2) to efficiently asymmetrisize the patterns.

(ii) The large peak located around $\theta=35°$ can be attributed to forward scattering along the atomic chains in this direction (ACB sequence) [direction 2, Fig. 5(b)]. But for the ABC sequence, the simulations show that a constructive interference between two forward-scattering directions at $\theta=19.5°$ (labeled 3) and 54.7° (labeled 4), ($-19.5°$ and $-54.7°$ for the ACB sequence), give rise to a peak around $\theta=35°$ ($\theta=-35°$).

The C 1*s* XPD patterns scanned in the same (11-20) azimuthal plane are shown in Figs. 7(a) and 7(b) for the 3×3 and $\sqrt{3}\times\sqrt{3}R30°$ surface reconstructions, respectively. We only will discuss the broad forward-scattering feature around $\theta=35°$. It is formed by two single structures near 30° and 40°. The last one is due to carbon atomic chains along the $\theta=35.25°$ direction (ACB sequence) or $-35.25°$ (ABC sequence). The close adjacent Si atomic chain along the same direction probably shifts this forward-scattering peak toward 40°, the silicon atoms being stronger scatterers than carbon. For the BCA sequence silicon scatterers are located at $\theta=29.5°$ [direction 3 in Fig. 5(a)] and contribute probably to the structure around 30°. As in the case of the Si 2*p* XPD patterns, no drastic dependence of the diffraction distributions are observed with the surface reconstructions and the experimental patterns are well reproduced by calculations relative to a bulk structure [Fig. 7(c)].

To sum up this part, we have shown that the XPD patterns relative to bulk components are completely insensitive to the reconstructions, whatever the probed core levels or azimuthal planes are. Due to rather high electron escape depths (around 20 Å), the XPS probing depth is around 60 Å and the contributing part of the surface reconstruction to the XPD signal becomes negligible. These results are contradictory to those of King *et al.*[23] who report XPD pattern variations for scanned bulk core-level peaks and attribute them to the 3×3 and $\sqrt{3}\times\sqrt{3}R30°$ reconstructions.

V. $6\sqrt{3}\times6\sqrt{3}R30°$ SURFACE RECONSTRUCTION

The insensitivity of the XPD patterns to the 3×3 and $\sqrt{3}\times\sqrt{3}R30°$ surface reconstructions is well established; we now examine the case of the $6\sqrt{3}\times6\sqrt{3}R30°$ reconstruction. The relevant Si 2*p* XPD patterns [Figs. 3(c) and 6(c)] remain similar to those of the two former reconstructions, but the convolution of the C 1*s* line by an important surface component S_1 [Fig. 1(f)] must now be taken into account in the XPD treatment. The use of a low pass energy (20 eV) enables us to perform B_1 and S_1 component deconvolutions at each polar angle, allowing separate XPD profiles for the bulk B_1 [Figs. 8(c) and 8(f)] and surface S_1 [Figs. 8(a) and 8(d)] components, respectively.

For the B_1 components we find again the characteristic XPD modulations of the substrate in the probed azimuthal planes. Thus, the bulk distributions Fig. 8(c) and 8(f) have to be compared to those of Figs. 7 and 4, respectively. This clearly attests to the relevance of our deconvolution in order to record the modulations of each component.

The new point concerns the XPD patterns of the S_1 surface component. In the (11-20) plane [Fig. 8(a)] we observe forward-scattering peaks near $\theta=0$, 20, 40, and 60° whereas $\theta=0$ and 70° features are obtained in the (10-10) plane.

On the basis of these structural observations, we can now try to determine the possible atomic structure leading to the $6\sqrt{3}\times6\sqrt{3}R30°$ reconstructed surface. As previously described, a lot of authors[4,5,11,25,26] using STM noticed a honeycomb structure attributed to a graphite layer. Its commensuration with the SiC substrate leads to a 6×6 surstructure.[21] Northrup and Neugebauer[15] concluded from their calculation that a Si adatom at the T_4 site for the $\sqrt{3}\times\sqrt{3}R30°$ reconstruction should be a very stable configuration with respect to the ideal surface and should explain the $6\sqrt{3}\times6\sqrt{3}R30°$ phase as a graphite monolayer on the $\sqrt{3}\times\sqrt{3}R30°$ surface. This idea was tentatively confirmed by Van Elsbergen, Kampen, and Mönch[7] with Auger-electron spectroscopy measurements.

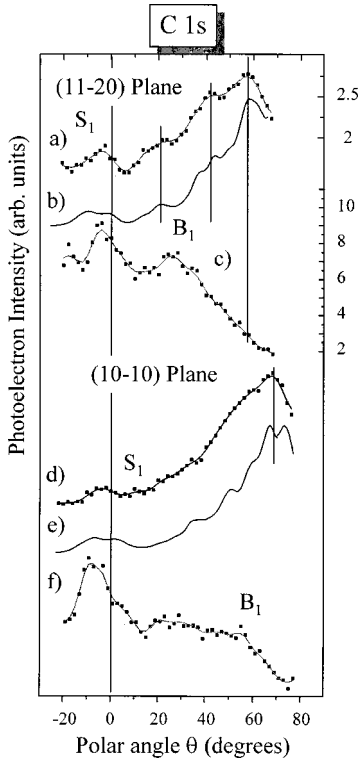

FIG. 8. XPD patterns of the S_1 (a and d) and B_1 (c and f) component convoluted in the C $1s$ core-level peak recorded on a $6\sqrt{3}\times6\sqrt{3}R30°$ reconstructed surface in the (11-20) and (10-10) azimuthal plane, respectively. Curves (b) and (e) are the results of simulated XPD modulations of the carbon atom at the last ending Si-C substrate bilayer with a reconstruction model which consists of a commensurable graphite layer on the top of a $\sqrt{3}\times\sqrt{3}R30°$ reconstructed surface with silicon adatoms at T_4 site. (See also the schematic representation in Fig. 9.)

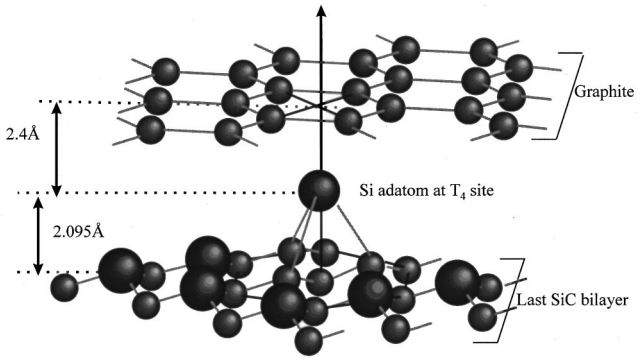

FIG. 9. Schematic representation of the proposed structural model for the $6\sqrt{3}\times6\sqrt{3}R30°$ reconstructed surface. It consists of a $\sqrt{3}\times\sqrt{3}R30°$ surface reconstruction with silicon or carbon adatoms at the T_4 sites capped by a graphite layer.

It is now admitted that a graphite layer is present at the top of the surface. With this hypothesis, the S_1 component should account for carbon atoms in a graphite plane. The first question is to determine whether the graphite layer is formed by one or more planes. In the case of a unique graphite plane, no scatterer would be seen in the $\langle 0001\rangle$ direction ($\theta=0°$), and no structured S_1 pattern should be observed. The forward-scattering peaks for the S_1 component in the XPD patterns [Figs. 8(a) and 8(d)] exclude this possibility. We have simulated two graphite planes arranged as in bulklike graphite. In the latter case a forward-scattering peak at $\theta=0°$ is expected together with another one, large and intense, located around $\theta=30°$ in the (11-20) azimuthal plane but no structure around $\theta=20°$ as experimentally observed. This also excludes the possibility of the presence of two graphite planes.

The correlation between the $\sqrt{3}\times\sqrt{3}R30°$ and $6\sqrt{3}\times6\sqrt{3}R30°$ surface reconstructions is now well established by STM.[3,5,20,21] Our preceding XPS characterizations confirm this point. We have observed two surface components S_1 and S_2 for the C $1s$ peak for the $\sqrt{3}\times\sqrt{3}R30°$ surface reconstruction and the same surface components for the $6\sqrt{3}\times6\sqrt{3}R30°$ surface reconstruction with an increase of the S_1 intensity. We noted that when the $\sqrt{3}\times\sqrt{3}R30°$ LEED pattern was taking place, the S_1 component intensity, first weak, increased with subsequent heating before the LEED pattern changed to the $6\sqrt{3}\times6\sqrt{3}R30°$ surface reconstruction. At this stage we suppose that the first C_6 rings of graphite can be formed on top of C-rich $\sqrt{3}\times\sqrt{3}R30°$ reconstructed surface zones. In order to develop a $6\sqrt{3}\times6\sqrt{3}R30°$ LEED pattern, large 6×6 zones of the surface must be covered by graphite planes. Following this idea, we have considered the structural model proposed by Northrup and Neugehauer[15] for the $6\sqrt{3}\times6\sqrt{3}R30°$ surface reconstruction, i.e., at the formation of a commensurable graphite plane on the top of the previously $\sqrt{3}\times\sqrt{3}R30°$. For this last reconstruction the authors proposed a silicon adatom at the T_4 site. The observed forward-scattering peak at $\theta=0°$ for the S_1 component [Figs. 8(a) and 8(d)] strongly suggests this model. Indeed, in this case, each carbon atom belonging to the last SiC substrate bilayer and beneath the T_4 adatoms $\sqrt{3}\times\sqrt{3}R30°$ reconstruction sites may now give rise to a forward scattering in the $\theta=0°$ direction (Fig. 9). Indeed, the other weak structures observed on the XPD pattern at greater polar angles cannot be explained only by an adatom at the T_4 site. Following the model of a $6\sqrt{3}\times6\sqrt{3}R30°$ reconstructed surface proposed by Northrup and Neugebauer,[15] we have considered an adatom at the T_4 site with a commensurable graphite layer on the top of them. The S_1 component is attributed to the graphite layer and, considering our XPD patterns, may also be attributed to the carbon atoms of the last SiC substrate bilayer situated just under the adatom at T_4 sites (Fig. 9). In order to explain the contribution of the S_1 component for these carbon atoms of the SiC surface, we consider that they are bonded with three carbon atoms supporting the adatom T_4. In this case the silicon atoms of the last SiC bilayer, bonded with the adatoms at the T_4 sites, are substituted by carbon atoms. These carbon atoms bonded with the adatom T_4 are back-bonded with carbon atoms of the substrate surface and can reasonably give the S_2 component observed in the C $1s$ peak. We have simulated this structural model. The required graphite lattice constant, necessary to match the $6\sqrt{3}\times6\sqrt{3}R30°$ cell of SiC exactly, is 2.464 Å. The distance between the adatom at the T_4 site and the last silicon substrate layer is set at 2.095 Å as considered by Northrup and Neugebauer.[15] The distance between the graphite layer and the Si adatom in the T_4 site is chosen to 2.4 Å (see Fig. 9). Reducing this distance gives rise, by simulation, to the same weak structures (near $\theta=20$ and 40°)

but shifted to higher polar angles for the (11-20) azimuthal plane. The simulation of the XPD modulation contributions of carbon emitters attributed to the S_1 component, i.e., each carbon atom of the SiC surface under adatom T_4 and those from the graphite overlayer, is represented in Figs. 8(b) and 8(e) for the two (11-20) and (10-10) azimuthal planes. We have experimentally measured the instrumental function giving rise to an increase of the signal intensity with increasing polar angles, by deposing an amorphous carbon monolayer with a carbon solid source on Si (substrate) and recording the XPD pattern of the C 1*s* core-level peak. After normalization this instrumental function has been added to the theoretical calculation in order to reproduce the observed photoemission intensity which increases at grazing angles and to realize a good comparison between experimental and theoretical XPD patterns. The weak structures near $\theta=20°$, 40°, and 60° for the (11-20) azimuthal plane are well reproduced by our simulation. For the other (10-10) azimuthal plane, the structure near $\theta=70°$ is also reproduced. We obtain a fairly good agreement between our simulation of the proposed structural model and the XPD pattern of the S_1 component. These results cannot definitively rule out other structural models proposed previously. Considering graphitic states as the result of a graphite layer on top of the $\sqrt{3}\times\sqrt{3}R30°$ reconstruction, the sufficiently intense scattering peak observed at $\theta=0°$ strongly suggests that, among the proposed structural models, an adatom in a T_4 site is the most favorable. It can either be carbon or silicon. In these two cases it is bonded with carbon atoms which may explain the absence of a surface component in the Si 2*p* peak for the $6\sqrt{3}\times6\sqrt{3}R30°$ surface reconstruction [Figs. 2(e) and 2(f)]. Our reasoning about the interpretation of the surface components S_1 and S_2 of the C 1*s* peak, far from fully rigorous, cannot clear up this point. However, Johansson, Owman, and Märtensson,[6] by synchrotron high resolution core-level examinations, have observed two surface components for the Si 2*p* peak. This strongly suggests that the adatoms at T_4 sites in our model are silicon ones.

VI. CONCLUSION

XPS and XPD characterizations of 6*H*-SiC(0001) substrates have been performed for different surface reconstructions (Si-rich 3×3, C-rich $\sqrt{3}\times\sqrt{3}R30°$, and $6\sqrt{3}\times6\sqrt{3}R30°$). A full set of experimental XPD patterns have been compared to simulations obtained by double-scattering calculation. The two (11-20) and (10-10) azimuthal planes have been well identified by this technique and each angular structure of the XPD patterns is well reflected by our calculations. No change of the XPD pattern with the reconstruction has been observed. In the last case of the $6\sqrt{3}\times6\sqrt{3}R30°$ reconstructed surface, the XPD pattern of each component of the C 1*s* core-level line is presented and a structural model is proposed. It consists of silicon adatoms at T_4 sites bonded with carbon atoms substituting silicon surface atoms at $\sqrt{3}\times\sqrt{3}R30°$ sites with a commensurable graphite layer on the top of them. A fairly good agreement between the experimental and calculated XPD modulations is obtained for this proposed structural model. Finally we demonstrate the possibility to elaborate a two-dimensional graphite surface layer. Compared to bulk graphite, such a system provides dimensionality reduction which may occasion fundamental interests such as, the study of two-dimensional plasmons.

ACKNOWLEDGMENTS

This work was financially supported by an ARA/LETI (CEA) grant. The authors are pleased to thank G. Gewinner and P. Wetzel for providing the XPD calculation program.

*Author to whom correspondence should be addressed. FAX: +33 (0) 0389336083. Electronic address: L. simon@univ-mulhouse.fr

[1] J. A. Powell, D. J. Larkin, P. B. Abel, L. Zhou, and P. Pirouz, in *Proceedings Silicon Carbide and Related Materials Conference, Kyoto, Japan, 1995*, IOP Conf. Proc. No. 142 (Institute of Physics, London, 1996), p. 77.

[2] A. J. Van Bommel, J. E. Crombeen, and A. Van Tooren, Surf. Sci. **48**, 463 (1975).

[3] F. Owman and P. Märtensson, J. Vac. Sci. Technol. B **14**, 933 (1996).

[4] T. Tsukamoto, M. Hirai, M. Kusaka, M. Iwami, T. Ozawa, T. Nagamura, and T. Nakata, Appl. Surf. Sci. **113/114**, 467 (1997).

[5] T. Tsukamoto, M. Hirai, M. Kusaka, M. Iwami, T. Ozawa, T. Nagamura, and T. Nakata, Surf. Sci. **371**, 316 (1997).

[6] L. I. Johansson, F. Owman, and P. Märtensson, Phys. Rev. B **53**, 13 793 (1996).

[7] V. Van Elsbergen, T. U. Kampen, and W. Mönch, Surf. Sci. **365**, 443 (1996).

[8] M. A. Kulakov, G. Henn, and B. Bullemer, Surf. Sci. **346**, 49 (1996).

[9] M. A. Kulakov, H. Hoster, G. Henn, and B. Bullemer, Mater. Sci. Eng., B **46**, 227 (1997).

[10] F. Owman and P. Märtensson, Surf. Sci. **330**, L639 (1995).

[11] L. Li and I. S. T. Tsong, Surf. Sci. **351**, 141 (1996).

[12] S. Nakanishi, H. Tokutaka, K. Nishimori, S. Kishida, and N. Ishiara, Appl. Surf. Sci. **41**, 44 (1989).

[13] R. Kaplan, Surf. Sci. **215**, 111 (1989).

[14] R. Gunnella, J. Y. Veuillen, A. Berthet, and T. A. Nguyen, Surf. Rev. Lett. **5**, 187 (1998).

[15] J. E. Northrup and J. Neugebauer, Phys. Rev. B **52**, R17 001 (1995).

[16] I. Forbeaux, J. M. Themlin, V. Langlais, L. M. Yu, H. Belkhir, and J. M. Debever, Surf. Sci. Lett. **5**, 193 (1998).

[17] L. I. Johansson, F. Owman, P. Märtensson, C. Persson, and U. Lindefelt, Phys. Rev. B **53**, 13 803 (1996).

[18] P. Badziag, Surf. Sci. **412/413**, 502 (1998).

[19] L. I. Johansson, F. Owman, and P. Märtensson, Phys. Rev. B **53**, 13 793 (1996).

[20] P. Heuell, M. A. Kulakov, V. F. Tsvetkov, and B. Bullemer, in *Silicon Carbide and Related Materials: Proceedings of the Fifth International Conference*, IOP Conf. Proc. No. 137 (Institute of Physics, London, 1994), p. 353.

[21] M. H. Tsai, C. S. Chang, J. D. Dow, and I. S. T. Tsong, Phys. Rev. B **45**, 1327 (1992).

[22] J. L. Bischoff, D. Dentel, and L. Kubler, Surf. Sci. **415**, 392 (1998).

[23] S. W. King, C. Ronning, R. F. Davis, R. S. Busby, and R. J. Nemanich, J. Appl. Phys. **84**, 6042 (1998).

[24] T. Jikimoto, T. Tsukamoto, A. Kinoshita, Y. Satoh, M. Hirai, M. Kusaka, M. Iwami, and T. Nakata, Appl. Surf. Sci. **117/118**, 794 (1997).
[25] V. Van Elsbergen, H. Nienhaus, and W. Mönch, Appl. Surf. Sci. **123/124**, 38 (1998).
[26] U. Starke, J. Schardt, J. Bernhardt, M. Franke, K. Reuter, H. Wedler, K. Heinz, J. Furthmüller, P. Käckel, and F. Bechstedt, Phys. Rev. Lett. **80**, 758 (1998).
[27] K. Reuter, J. Schardt, J. Bernhardt, H. Wedler, U. Starke, and K. Heinz, Phys. Rev. B **58**, 10 806 (1998).
[28] P. Badziag, Surf. Sci. **402**, 822 (1998).
[29] C. S. Fadlay, Prog. Surf. Sci. **16**, 275 (1984).
[30] L. Simon, L. Kubler, A. Ermolieff, and T. Billon, Phys. Rev. B **60**, 5673 (1999).
[31] S. Juillaguet, L. Kubler, M. Diani, J. L. Bischoff, G. Gewinner, P. Wetzel, and N. Bécourt, Surf. Sci. **339**, 363 (1995).